CrystEngComm

PAPER

View Article Online
View Journal | View Issue

Five MOFs with different topologies based on anthracene functionalized tetracarboxylic acid: syntheses, structures, and properties†

Cite this: *CrystEngComm*, 2014, **16**, 2917

Fuling Liu,[a] Liangliang Zhang,[b] Rongming Wang,*[b] Jie Sun,[a] Jie Yang,[a] Zhen Chen,[a] Xingpo Wang*[a] and Daofeng Sun*[ab]

Received 24th October 2013,
Accepted 27th November 2013

DOI: 10.1039/c3ce42152j

www.rsc.org/crystengcomm

Five coordination polymers based on 5,5′-(2,3,6,7-tetramethoxyanthracene-9,10-diyl)diisophthalic acid (H_4L^{OMe}): $[Mn_4(L^{OMe})(OAc)_2(\mu_3\text{-}OH)_2(NMP)_4(H_2O)_2]\cdot 2H_2O$ (**1**), $[Ni_2(L^{OMe})_{0.5}(H_2L^{OMe})_{0.5}(\mu_3\text{-}OH)(H_2O)_3]\cdot 6H_2O$ (**2**), $[Cd_2(L^{OMe})(H_2O)_2(NMP)]\cdot 2DMF\cdot NMP\cdot H_2O$ (**3**), $[Co_2(L^{OMe})(H_2O)_2]\cdot 2NMP\cdot DMA\cdot 2H_2O$ (**4**), $[Zn_2(L^{OMe})(H_2O)_2]\cdot 2NMP\cdot 2H_2O\cdot DOE$ (**5**) (NMP = *N*-methylpyrrolidone, DMF = *N*,*N*′-dimethylformamide, DMA = *N*,*N*′-dimethylacetamide, DOE = 1,4-dioxane) were prepared by solvothermal methods and characterized by elemental analysis (EA), single-crystal X-ray crystallography, powder X-ray diffraction (PXRD), infrared spectroscopy (IR), and thermogravimetric analyses (TGA). X-ray crystallography analysis shows that complex **1** bears a two-dimensional (2D) (4,4) network based on tetranuclear secondary building units, which are further assembled into a three-dimensional supramolecular structure *via* π···π stacking interaction; complex **2** displays a 3D framework with **fsc** topology based on 2D 4^4-**sql** layers and tetranuclear SBUs; complex **3** reveals a 3D **PtS** network *via* the L^{OMe} bridging dimetal $\{Cd_2O_{11}\}$ units; complexes **4** and **5** possess 3D open frameworks with a rarely reported 3-nodal (4,4,4)-connected **nou** network. Moreover, magnetic susceptibility measurement of complexes **1** and **2** confirm the presence of magnetic exchange coupling among the metal ions of tetranuclear clusters, and fluorescent spectra of complexes **1**, **3** and **5** show emission signals in the blue region.

1. Introduction

Metal–organic frameworks (MOFs) with infinite one-, two-, or three-dimensional (1D, 2D, or 3D) structures are assembled with metal ions or polynuclear clusters as nodes and organic ligands as linkers.[1] Recently, the design and construction of MOFs have attracted increasing attention, and numerous MOFs have been reported not only because of their intriguing variety of crystal structures and topologies,[2] but also for their potential applications in gas storage, catalysis, drug delivery, luminescence, nonlinear optics, magnetism and sensing.[3] To the best of our knowledge, it is still a significant challenge to precisely control the MOF structure from a self-assembly system because many synthetic parameters such as metal ions, organic ligands, solvent systems, pH, temperature and metal-to-ligand ratio may have a non-negligible influence on the self-assembly process.[4] Without a doubt, the tactical design and rational use of the characteristic ligand are all-important among these factors. The rigidity, length, coordination modes, functional groups, or substituents of organic ligands have important effects on the final structures of MOFs.[5] In particular, the aromatic polycarboxylate ligands can serve as excellent candidates for building highly connected, self-penetrating, helical coordination polymers or frameworks due to their versatile bridging fashions and bent backbones.[6,7]

It is well known that rigid, elongated and widened tetracarboxylate acids have often been employed as bridging ligands to construct MOFs, because this kind of ligand can act as a rectangular-planar 4-connected node, and the synthesized compounds have numerous applications.[8] However, the type and size of substituent groups of organic ligands have significant effects on the character of the ligand, which also can ultimately determine the structure of the product. In this work, a new tetracarboxylic ligand (5,5′-(2,3,6,7-tetramethoxyanthracene-9,10-diyl)diisophthalic

[a] *Key Lab of Colloid and Interface Chemistry, Ministry of Education, School of Chemistry and Chemical Engineering, Shandong University, Jinan, 250100, PR China. E-mail: dfsun@sdu.edu.cn, xpw6@sdu.edu.cn*
[b] *College of Science, China University of Petroleum (East China), Qingdao, Shandong 266555, People's Republic of China. E-mail: rmwang@upc.edu.cn*

† Electronic supplementary information (ESI) available: Detailed synthesis procedure, powder X-ray diffraction (PXRD) patterns, TGA and IR spectra for **1**–**5**. CCDC 967536–967540 for **1**–**5**. For ESI and crystallographic data in CIF or other electronic format see DOI: 10.1039/c3ce42152j

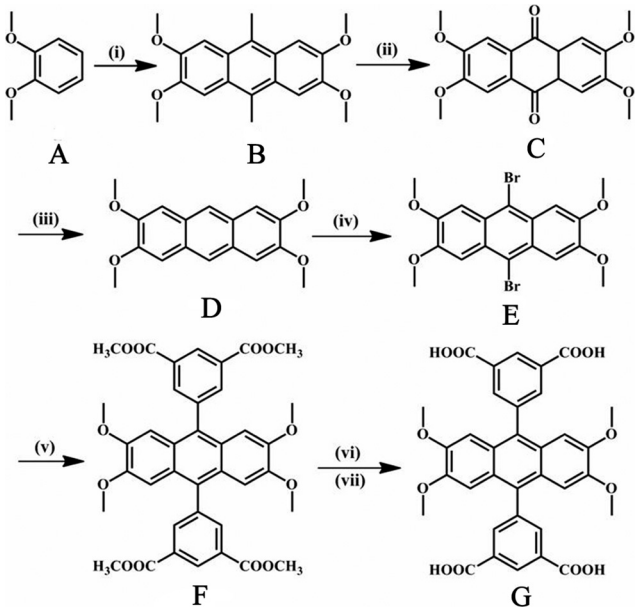

Scheme 1 Synthesis route for H_4L^{OMe}. (i) MeCHO, H_2SO_4, –10 °C; (ii) $Na_2Cr_2O_7$, HAc, reflux; (iii) Zn, NaOH 8–10% aq, 100 °C; (iv) Br_2, CCl_4 reflux; (v) (3,5-bis(methoxycarbonyl)phenyl)boronic acid, $Pd(PPh_3)_4$, CsF, DME, 90 °C; (vi) THF, MeOH; (vii) HCl, pH = 1.

acid, H_4L^{OMe}) was synthesized as shown in Scheme 1. Undoubtedly, the methoxy substituent has an important influence on the properties of the ligand such as width, solubility, effects as an electron donor or acceptor, hydrophobic character, possibility of additional intermolecular interactions and coordination mode of the ligand. At present, five metal–organic frameworks $[Mn_4(L^{OMe})(OAc)_2(\mu_3\text{-}OH)_2(NMP)_4(H_2O)_2]\cdot 2H_2O$ (**1**), $[Ni_2(L^{OMe})_{0.5}(H_2L^{OMe})_{0.5}(\mu_3\text{-}OH)(H_2O)_3]\cdot 6H_2O$ (**2**) $[Cd_2(L^{OMe})(H_2O)_2(NMP)]\cdot 2DMF\cdot NMP\cdot H_2O$ (**3**), $[Co_2(L^{OMe})(H_2O)_3]\cdot 2NMP\cdot DMA\cdot H_2O$ (**4**), and $[Zn_2(L^{OMe})(H_2O)_2]\cdot 2NMP\cdot 2H_2O\cdot DOE$ (**5**) were obtained by changing the metal ions, temperatures and solvent systems and characterized by single-crystal X-ray crystallography, powder X-ray diffraction (PXRD), elemental analysis (EA), infrared spectroscopy (IR), and thermogravimetric analyses (TGA). The results show that these complexes have interesting structural topologies. Meanwhile, fluorescence properties of complexes **1**, **3** and **5** and magnetic susceptibilities of complexes **1** and **2** were also studied and analyzed.

2. Experimental

2.1. Materials and methods

All chemicals and solvents used in the syntheses were of analytical grade and used without further purification. H_4L^{OMe} was synthesized by a series of redox and Suzuki coupling reactions. The purity of the ligand was determined by ^1H NMR in d^6-DMSO (see ESI†). Powder X-ray diffraction measurements were performed with a Bruker AXS D8 Advance. The FT-IR spectra were recorded in the range 4000–400 cm^{-1} on a Nicolet 330 FTIR spectrometer using the KBr pellet method. C, H, and N analyses were carried out on a PerkinElmer 240 elemental analyzer. Thermogravimetric analysis (TGA) experiments were performed using a PerkinElmer TGA instrument (heating rate of 10 °C min^{-1}; nitrogen stream) from room temperature to 800 °C. Photoluminescence spectra were measured on a F-280 fluorescence spectrophotometer. Variable-temperature magnetic susceptibilities were measured with an MPMS XL-7 superconducting quantum interference device (SQUID) magnetometer. Diamagnetic corrections were made with Pascal's constants for all constituent atoms.

2.2. Preparation of complexes 1–5

2.2.1. Preparation of $[Mn_4(L^{OMe})(OAc)_2(\mu_3\text{-}OH)_2(NMP)_4(H_2O)_2]\cdot 2H_2O$ (1). A mixture of $Mn(OAc)_2\cdot 4H_2O$ (20mg, 0.13 mmol) and H_4L^{OMe} (2.5 mg, 0.004 mmol) was dissolved in NMP (*N*-methylpyrrolidone)–DEF (diethylforamide)–H_2O mixed solvent (1 mL, v/v/v = 1/1/1). Then, the solution was sealed in a pressure-resistant glass tube, slowly heated to 75 °C from room temperature in 8 hours, kept at 75 °C for 33 hours, and then slowly cooled to 30 °C in 10 hours. The formed brown crystals were collected and dried in the air. (Yield: 50%, based on manganese). Elemental analysis (%): calcd. for $C_{58}H_{74}Mn_4N_4O_{26}$: C, 47.62; H, 5.10; N, 3.83. Found: C, 48.43; H, 4.934; N, 3.18. IR (KBr): ν (cm^{-1}) = 3478.68 (w), 2955.80 (w), 1656.11 (s), 1582.76 (s), 1487.77 (m), 1431.35 (s), 1372.10 (s), 1239.50 (m), 1150.16 (w), 1012.85 (w), 742.00 (w), 664.89 (w), 449.53 (w).

2.2.2. Preparation of $[Ni_2(L^{OMe})_{0.5}(H_2L^{OMe})_{0.5}(\mu_3\text{-}OH)(H_2O)_3]\cdot 6H_2O$ (2). A mixture of $Ni(NO_3)_2\cdot 6H_2O$ (20 mg, 0.07 mmol) and H_4L^{OMe} (2.5 mg, 0.004 mmol) was dissolved in NMP (*N*-methylpyrrolidone)–DMA–H_2O mixed solvent (1 mL, v/v/v = 1/1/1). Then, the solution was sealed in a pressure-resistant glass tube, slowly heated to 130 °C from room temperature in 8 hours, kept at 130 °C for 50 hours, and then slowly cooled to 30 °C in 13 hours. The formed green crystals were collected and dried in the air. (Yield: 57%, based on Ni). Elemental analysis (%): calcd. for $C_{34}H_{42}Ni_2O_{22}$: C, 44.38; H, 4.60. Found: C, 43.16; H, 4.80. IR (KBr): ν (cm^{-1}) = 3416.59 (w), 2940.02 (w), 1620.51 (s), 1495.09 (s), 1429.69 (s), 1363.56 (s), 1239.60 (s), 1157.44 (w), 1015.97 (w), 851.71 (w), 748.00 (m).

2.2.3. Preparation of $[Cd_2(L^{OMe})(H_2O)_2(NMP)]\cdot 2DMF\cdot NMP\cdot H_2O$ (3). A mixture of $Cd(NO_3)_2\cdot 4H_2O$ (20 mg, 0.065 mmol) and H_4L^{OMe} (2.5 mg, 0.004 mmol) was dissolved in NMP (*N*-methylpyrrolidone)–DMF–H_2O mixed solvent (1 mL, v/v/v = 1/1/1). Then, the solution was sealed in a pressure-resistant glass tube, slowly heated to 75 °C from room temperature in 8 hours, kept at 75 °C for 33 hours, and then slowly cooled to 30 °C in 10 hours. The formed brown crystals were collected and dried in the air. (Yield: 43%, based on Cd). Elemental analysis (%): calcd. for $C_{50}H_{66}Cd_2N_4O_{19}$: C, 47.97; H, 5.31; N, 4.48. Found: C, 48.83; H, 4.750; N, 4.27. IR (KBr): ν (cm^{-1}) = 3522.95 (w), 2932.09 (w), 1661.26(s),

1493.90 (s), 1434.26 (s), 1363.76 (s), 1236.39 (s), 1156.84 (m), 1101.03 (w), 1016.00 (m), 848.68 (w), 744.37 (s), 664.08 (w), 594.48 (w), 441.02 (w).

2.2.4. Preparation of $[Co_2(L^{OMe})(H_2O)_2]\cdot 2NMP\cdot DMA\cdot 2H_2O$ (4). Synthesis of **4** was similar to that of **2**, but the $Ni(NO_3)_2\cdot 6H_2O$ was replaced by $Co(NO_3)_2\cdot 6H_2O$ (20 mg, 0.07 mmol). Dark red crystals of **4** were obtained in 62% yield. Elemental analysis (%): calcd. for $C_{48}H_{57}Co_2O_{19}N_3$: C, 52.51; H, 5.23; N, 3.83. Found: C, 50.86; H, 5.05; N, 3.32. IR (KBr): ν (cm^{-1}) = 3424 (w), 2946.83 (w), 1638.65 (s), 1494.92 (s), 1432.68 (s), 1368.97 (s), 1238.57 (s), 1158.61 (m), 1016.65 (w), 848.50 (w), 748.28 (m), 462.46 (w).

2.2.5. Preparation of $[Zn_2(L^{OMe})(H_2O)_2]\cdot 2NMP\cdot 2H_2O\cdot DOE$ (5). A mixture of $Zn(NO_3)_2\cdot 6H_2O$ (20 mg, 0.067 mmol) and H_4L^{OMe} (2.5 mg, 0.004 mmol) was dissolved in NMP (*N*-methylpyrrolidone)–1,4-dioxane–H_2O mixed solvent (1 mL, v/v/v = 1/1/1). Then, the solution was sealed in a pressure-resistant glass tube, slowly heated to 130 °C from room temperature in 5 hours, kept at 130 °C for 50 hours, and then slowly cooled to 30 °C in 13 hours. The formed brown crystals were collected and dried in the air. (Yield: 64%, based on Zn). Elemental analysis (%): calcd. for $C_{48}H_{56}Zn_2N_2O_{20}$: C, 51.86; H, 5.08; N, 2.52. Found: C, 50.40; H, 4.848; N, 2.01. IR (KBr): ν (cm^{-1}) = 3521.46 (w), 2954.76 (w), 2856.22 (w), 1642.73 (s), 1494.89 (s), 1434.88 (s), 1369.04 (s), 1239.11 (s), 1158.88 (w), 1116.35 (w), 1016.29 (w), 848.43 (w), 748.97 (m), 464.71 (w).

2.3. X-ray crystallography

Single crystals of the complexes **1–5** with appropriate dimensions were chosen under an optical microscope and quickly coated with high vacuum grease (Dow Corning Corporation) before being mounted on a glass fiber for data collection. Diffraction data were collected with a Bruker APEX II CCD single-crystal X-ray diffractometer with a graphite monochromated Mo-Kα radiation (λ = 0.71073 Å) source at room temperature. All absorption corrections were applied using the multiscan program SADABS. In all cases, the highest possible space group was chosen. All structures were solved by direct methods using the SHELXS-97[9] program of the SHELXTL package and refined by the full-matrix least-squares method with SHELXL-97.[10] Atoms were located from iterative examination of difference *F*-maps following least squares refinements of the earlier models. Hydrogen atoms were placed in calculated positions and included as riding atoms with isotropic displacement parameters 1.2–1.5 times U_{eq} of the attached C atoms. There are some solvent accessible void volumes in the crystals of **2–5** which are occupied by highly disordered solvent molecules. No satisfactory disorder model could be achieved, and therefore the SQUEEZE program implemented in PLATON[11] was used to remove these electron densities. All structures were examined using the Addsym subroutine of PLATON to assure that no additional symmetry could be applied to the models. For complex **3**, the atoms of the NMP ligand were modeled and refined

Table 1 Crystal data for **1–5**[a]

Compound	1	2	3	4	5
Empirical formula	$C_{58}H_{74}Mn_4N_4O_{26}$	$C_{34}H_{42}Ni_2O_{22}$	$C_{50}H_{66}Cd_2N_4O_{19}$	$C_{48}H_{57}Co_2O_{19}N_3$	$C_{48}H_{56}Zn_2N_2O_{20}$
Formula weight	1462.97	920.10	1251.87	1097.83	1111.69
T (K)	298(2)	298(2)	298(2)	298(2)	298(2)
Crystal system	Triclinic	Triclinic	Monoclinic	Monoclinic	Monoclinic
Space group	$P\bar{1}$	$P\bar{1}$	$P2_1/c$	$P2_1/c$	$P2_1/c$
a/Å	8.792(4)	11.080(3)	15.4676(17)	10.168(3)	10.107(4)
b/Å	11.024(5)	16.583(4)	13.1962(15)	18.035(5)	18.338(7)
c/Å	16.479(7)	16.600(4)	26.497(3)	27.054(8)	27.084(11)
α/°	84.580(7)	68.533(5)	90	90	90
β/°	85.459(7)	89.208(4)	98.729(2)	99.321(5)	99.285(8)
γ/°	78.893(7)	89.167(4)	90	90	90
V/Å^3	1557.0(11)	2837.9(13)	5345.8(10)	4896(3)	4954(3)
Z	1	2	4	4	4
ρ_{calc} mg mm^{-3}	1.560	1.077	1.555	1.489	1.490
μ/mm^{-1}	0.881	0.724	0.873	0.759	1.049
F(000)	758	956	2568	2288	2312
Reflections collected	7729	13 700	25 944	24 112	28 358
Independent reflections	5443 [R(int) = 0.0325]	9855 [R(int) = 0.0342]	9382 [R(int) = 0.0393]	8614 [R(int) = 0.0440]	11 147 [R(int) = 0.0649]
Parameters	421	476	479	452	457
Goodness-of-fit on F^2	1.029	0.983	1.033	1.073	0.860
Final R indexes [$I > 2\sigma(I)$]	R_1 = 0.0659, wR_2 = 0.1601	R_1 = 0.0555, wR_2 = 0.1564	R_1 = 0.0412, wR_2 = 0. 0.1128	R_1 = 0.0525, wR_2 = 0.1531	R_1 = 0.0492, wR_2 = 0.1216
Final R indexes [all data]	R_1 = 0.1019, wR_2 = 0.1833	R_1 = 0.0844, wR_2 = 0.1662	R_1 = 0.0551, wR_2 = 0.1197	R_1 = 0.0659, wR_2 = 0.1599	R_1 = 0.0896, wR_2 = 0.1216
Largest diff. peak/hole /e Å^{-3}	0.844/−0.677	0.782/−0.642	1.853/−0.611	1.633/−0.523	0.785/−0.542

[a] $R_1 = \sum||F_o| - |F_c||/\sum|F_o|$, $wR_2 = [\sum w(F_o^2 - F_c^2)^2]/\sum w(F_o^2)^2]^{1/2}$.

Table 2 Selected bond lengths (Å) and angles (°) for 1–5

Complex 1[a]					
Mn1–O4^{i}	2.146 (4)	Mn1–O11^{ii}	2.165 (4)	Mn1–O2	2.174 (4)
Mn1–O8	2.206 (5)	Mn1–O9	2.323 (4)	Mn1–O11	2.188 (3)
Mn2–O11^{ii}	2.160 (4)	Mn2–O9	2.239 (4)	Mn2–O7	2.240 (4)
Mn2–O3^{iii}	2.088 (4)	Mn2–O1	2.114 (4)	Mn2–O1W	2.253 (5)
O4^{i}–Mn1–O11	103.87 (14)	O2–Mn1–O9	83.30 (15)	O4^{i}–Mn1–O2	81.63 (15)
O4^{i}–Mn1–O8	87.15 (19)	O11^{ii}–Mn2–O9	79.02 (15)	O1–Mn2–O11^{ii}	97.10 (16)
O11^{ii}–Mn1–O9	77.08 (14)	O11–Mn1–O9	90.85 (14)	O3^{iii}–Mn2–O11^{ii}	93.74 (14)
O1–Mn2–O7	86.68 (17)	O11^{ii}–Mn2–O1W	84.86 (17)	O3^{iii}–Mn2–O7	83.10 (16)
Complex 2[b]					
Ni1–O13^{i}	2.025 (2)	Ni1–O1^{i}	2.050 (3)	Ni1–O8^{i}	2.051 (3)
Ni1–O3^{ii}	2.056 (3)	Ni1–O13	2.057 (2)	Ni1–O3W	2.130 (3)
Ni2–O13	1.975 (2)	Ni2–O2	2.027 (3)	Ni2–O7	2.044 (3)
Ni2–O4^{ii}	2.071 (3)	Ni2–O2W	2.094 (3)	Ni2–O1W	2.112 (5)
O13^{i}–Ni1–O1^{i}	99.01 (11)	O13^{i}–Ni1–O13	80.76 (11)	O1^{i}–Ni1–O3^{ii}	88.12 (11)
O8^{i}–Ni1–O13	89.49 (11)	O3^{ii}–Ni1–O13	92.27 (11)	O3^{ii}–Ni1–O3W	87.57 (12)
O2–Ni2–O2W	84.84 (13)	O13–Ni2–O2	95.34 (11)	O13–Ni2–O4^{ii}	93.08 (10)
O4^{ii}–Ni2–O2W	86.60 (13)	O2–Ni2–O1W	87.17 (17)	O2–Ni2–O7	91.60 (14)
Complex 3[c]					
Cd1–O1	2.218 (3)	Cd1–O7	2.255 (3)	Cd1–O10^{i}	2.274 (3)
Cd1–O3^{ii}	2.299 (3)	Cd1–O8	2.440 (3)	Cd1–O9^{i}	2.607 (3)
Cd1–O4^{ii}	2.617 (3)	Cd2–O2	2.232 (3)	Cd2–O13	2.242 (3)
Cd2–O1W	2.245 (3)	Cd2–O2W	2.265 (3)	Cd2–O10^{i}	2.297 (3)
Cd2–O4^{ii}	2.304 (3)				
O1–Cd1–O7	104.82 (11)	O1–Cd1–O9^{i}	90.13 (11)	O7–Cd1–O8	56.35 (10)
O8–Cd1–O4^{ii}	96.78 (10)	O10^{i}–Cd1–O8	97.14 (10)	O1–Cd1–O10^{i}	93.78 (11)
O1–Cd1–O4^{ii}	101.95 (11)	O3^{ii}–Cd1–O4^{ii}	52.33 (10)	O3^{ii}–Cd1–O8	96.75 (11)
O2–Cd2–O10^{i}	91.40 (11)	O13–Cd2–O10^{i}	89.33 (12)	O13–Cd2–O2W	87.08 (14)
O2–Cd2–O2W	91.92 (13)	O2–Cd2–O1W	90.35 (15)	O2–Cd2–O4^{ii}	87.98 (13)
Complex 4[d]					
Co1–O8^{i}	1.928 (3)	Co1–O4^{ii}	2.014 (2)	Co2–O2W	2.110 (3)
Co1–O6	1.933 (3)	Co2–O7^{i}	1.978 (3)	Co2–O1W	1.923 (7)
Co1–O1	1.966 (2)	Co2–O5	1.983 (3)	Co2–O2	2.041 (2)
Co1–O3^{ii}	2.298 (2)				
O8^{i}–Co1–O6	139.82 (14)	O8^{i}–Co1–O4^{ii}	102.62 (12)	O8^{i}–Co1–O1	96.25 (13)
O6–Co1–O4^{ii}	109.88 (12)	O1–Co1–O3^{ii}	166.05 (10)	O4^{ii}–Co1–O3^{ii}	59.79 (9)
O1W–Co2–O7^{i}	140.3 (2)	O1W–Co2–O5	105.3 (2)	O7^{i}–Co2–O5	113.09 (15)
O1W–Co2–O2	87.9 (3)	O7^{i}–Co2–O2	97.73 (13)	O5–Co2–O2	95.80 (12)
O7^{i}–Co2–O2W	86.37 (14)	O5–Co2–O2W	89.47 (12)	O2–Co2–O2W	171.41 (12)
Complex 5[e]					
Zn1–O7	1.944 (3)	Zn1–O9^{i}	1.956 (3)	Zn1–O4^{ii}	1.963 (2)
Zn1–O2	2.012 (2)	Zn1–O1	2.304 (3)	Zn2–O10^{i}	1.943 (3)
Zn2–O8	1.945 (3)	Zn2–O1W	1.965 (3)	Zn2–O3^{ii}	2.062 (3)
Zn2–O2W	2.138 (3)				
O2–Zn1–O1	59.88 (10)	O7–Zn1–O1	87.74 (11)	O7–Zn1–O4^{ii}	97.25 (12)
O9^{i}–Zn1–O4^{ii}	98.08 (12)	O9^{i}–Zn1–O1	90.93 (11)	O7–Zn1–O2	112.30 (12)
O4^{ii}–Zn1–O2	101.90 (11)	O9^{i}–Zn1–O2	106.10 (12)	O7–Zn1–O9^{i}	134.35 (12)
O4^{ii}–Zn1–O1	161.46 (10)	O10^{i}–Zn2–O8	132.22 (12)	O10^{i}–Zn2–O1W	118.78 (17)
O8–Zn2–O1W	108.19 (16)	O10^{i}–Zn2–O3^{ii}	94.11 (14)	O8–Zn2–O3^{ii}	96.02 (12)
O1W–Zn2–O3^{ii}	88.74 (12)	O10^{i}–Zn2–O2W	84.44 (13)	O8–Zn2–O2W	91.24 (11)
O1W–Zn2–O2W	84.51 (13)	O3^{ii}–Zn2–O2W	171.34 (11)		

[a] Symmetry codes: (i) $-x, -y, -z+1$; (ii) $-x, -y+1, -z+1$; (iii) $x, y+1, z$; (iv) $x, y-1, z$; (v) $-x, -y, -z$. [b] Symmetry codes: (i) $-x+1, -y+2, -z+1$; (ii) $x+1, y, z$; (iii) $-x, -y+1, -z+1$; (iv) $-x+1, -y+1, -z+2$; (v) $x-1, y, z$. [c] Symmetry codes: (i) $-x+1, y-1/2, -z+1/2$; (ii) $-x, y+1/2, -z+1/2$; (iii) $-x, y-1/2, -z+1/2$; (iv) $-x+1, y+1/2, -z+1/2$; (v) $-x, -y+1, -z$; (vi) $-x+1, -y+2, -z$. [d] Symmetry codes: (i) $-x+1, y-1/2, -z+1/2$; (ii) $x-1, y, z$. [e] Symmetry codes: (i) $-x+1, y+1/2, -z+1/2$; (ii) $x+1, y, z$; (iii) $x-1, y, z$; (iv) $-x, -y+2, -z+1$; (v) $-x+1, -y+1, -z+1$; (vi) $-x+1, y-1/2, -z+1/2$.

isotropically. Crystallographic data and experimental details for structural analyses for 1–5 are summarized in Table 1, and the selected bond lengths and bond angles are listed in Table 2.

3. Result and discussion

3.1. Synthesis and general characterization

All crystallization of complexes **1–5** were obtained under similar reaction conditions by solvothermal methods, which have been proven to be an effective and powerful technique for the self-assembly of MOFs.[12] By changing metal ions and solvents at different temperatures, the crystals suitable for the single-crystal X-ray diffraction analysis were finally obtained after cooling to room temperature. All complexes are stable in the solid state upon extended exposure to air and they have poor solubility in common organic solvents.

Powder X-ray diffraction (PXRD) has been used to check the phase purity of the bulk samples in the solid state. The measured PXRD patterns of complexes **1–5** closely match the simulated ones generated from the respective single-crystal X-ray data by using the Mercury 3.2 program (Fig. S2, ESI†), indicative of pure products. The dissimilarities in intensity may be due to the preferred orientation of the crystalline powder samples. The IR spectra of complexes **1–5** also show characteristic absorption bands, which are mainly attributed to the asymmetric (ν_{as}: *ca.* 1600 cm^{-1}) and symmetric (ν_s: *ca.* 1385 cm^{-1}) stretching vibrations of the carboxylic groups.

3.2. Structure descriptions

3.2.1. Structure description of $[Mn_4(L^{OMe})(OAc)_2(\mu_3\text{-}OH)_2(NMP)_4(H_2O)_2]\cdot 2H_2O$ (1). The single-crystal X-ray analysis reveals that complex **1** crystallizes in the triclinic $P\bar{1}$ space group and exhibits a two-dimensional framework based on tetranuclear manganese(II) clusters. Complex **1** consists of two Mn^{II} ions, half a L^{OMe} ligand, two coordinated NMP molecules, one acetate, one coordinated water and one μ_3-OH group in its asymmetric unit. Both of the Mn(II) atoms show octahedral geometry. The Mn1 atom is coordinated to two carboxylate oxygen atoms from two different L^{OMe} ligands, one oxygen atom of NMP, one oxygen atom of acetate and two μ_3-OH groups. The Mn2 atom is bonded to two carboxylate oxygen atoms from two different L^{OMe} ligands, and another four oxygen atoms from NMP, acetate, hydroxyl and H_2O, respectively (Fig. 1a). The Mn–O distances range from 2.088(4) to 2.323(4) Å, and the O–Mn–O bond angles range from 77.08(14) to 173.69(13)°. Two Mn(II) atoms are connected by one bidentate carboxylate, one acetate and one hydroxyl to generate a Mn_2 dimer, which is further linked through a pair of hydroxyls to form a Mn_4 cluster. The Mn_4 cluster lies on a crystallographic inversion centre, resulting in an exactly planar square array of Mn(II) atoms (Fig. 1b). The carboxylates of L^{OMe} connect the Mn_4 clusters with a bidentate mode to generate a 2D layer along the *bc* plane.

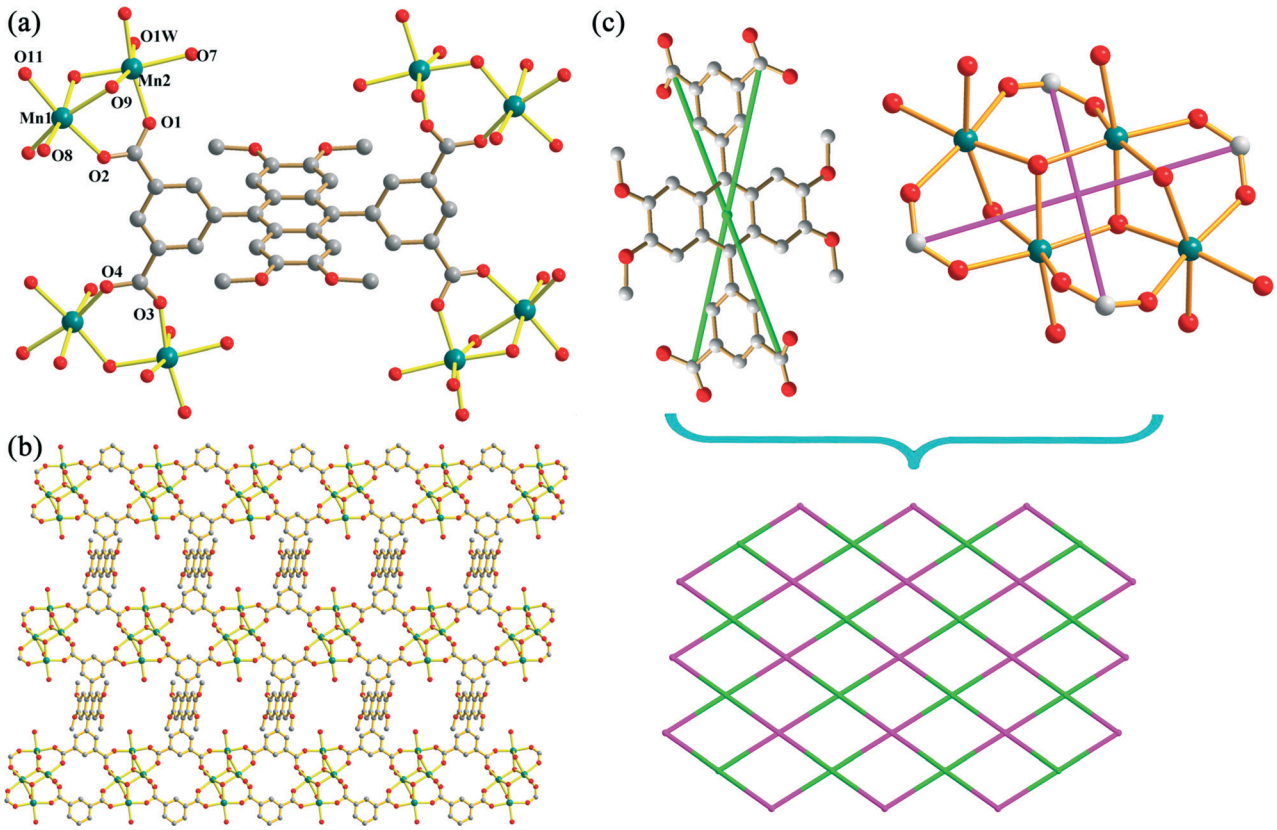

Fig. 1 (a) The coordination environment of Mn(II) ions in **1** (hydrogen atoms omitted for clarity). (b) The 2D layer linked by tetranuclear manganese clusters (NMP molecules are omitted for clarity). (c) Schematic representation of the (4^4)-**sql** layer connected topology. (Symmetry codes: (i) $-x+1, -y+1, -z+2$; (ii) $x, y-1, z$; (iii) $x, y+1, z$; (iv) $-x+1, -y+2, -z+1$).

Topologically, the individual 2-dimensional layer-like motif with the Schläfli symbol of $4^4{\cdot}6^2$ represents a 4-connected topology type (Fig. 1c). In **1**, the Mn_4 cluster (SBU) is simplified as a 4-connected node, and the L^{OMe} ligand is also regarded as a 4-connected node. Furthermore, the adjacent 2D layers are arranged into a 3D supramolecular framework by weak layer-to-layer hydrogen bonds (O11–H11···O2W = 2.774(16), O2W–H2W*A*···O10 = 2.717(17), O1W–H1W*B*···$O10^{vi}$ = 2.671(10) and O2W–H2W*B*···$O10^{vii}$ = 2.830(17), π···π stacking interactions and C–H···π interactions. Unfortunately, the void space of the cavity is occupied in the crystal by coordinated NMP molecules.

3.2.2. Structure description of $[Ni_2(L^{OMe})_{0.5}(HL^{OMe})_{0.5}(\mu_3\text{-}OH)(H_2O)_3]{\cdot}6H_2O$ (2). Structural analysis indicates that complex **2** is also a 3D framework with **fsc** topology and crystallizes in the triclinic $P\bar{1}$ space group. The asymmetric unit consists of two Ni(II), two halves of the ligand, three coordinated water molecules and one μ_3-OH group. As shown in Fig. 2a, the pairs of metal ions all adopt distorted octahedral geometries. Ni1 is coordinated to three carboxylate O atoms from three different ligands (Ni1–$O1^{i}$ = 2.050(3), Ni1–$O3^{ii}$ = 2.056(3), Ni1–$O8^{i}$ = 2.051(3) Å), two O atoms of μ_3-OH groups (Ni1–$O13^{i}$ = 2.025 (2), Ni1–O13 = 2.057 (2) Å) and one O atom from a coordinated water

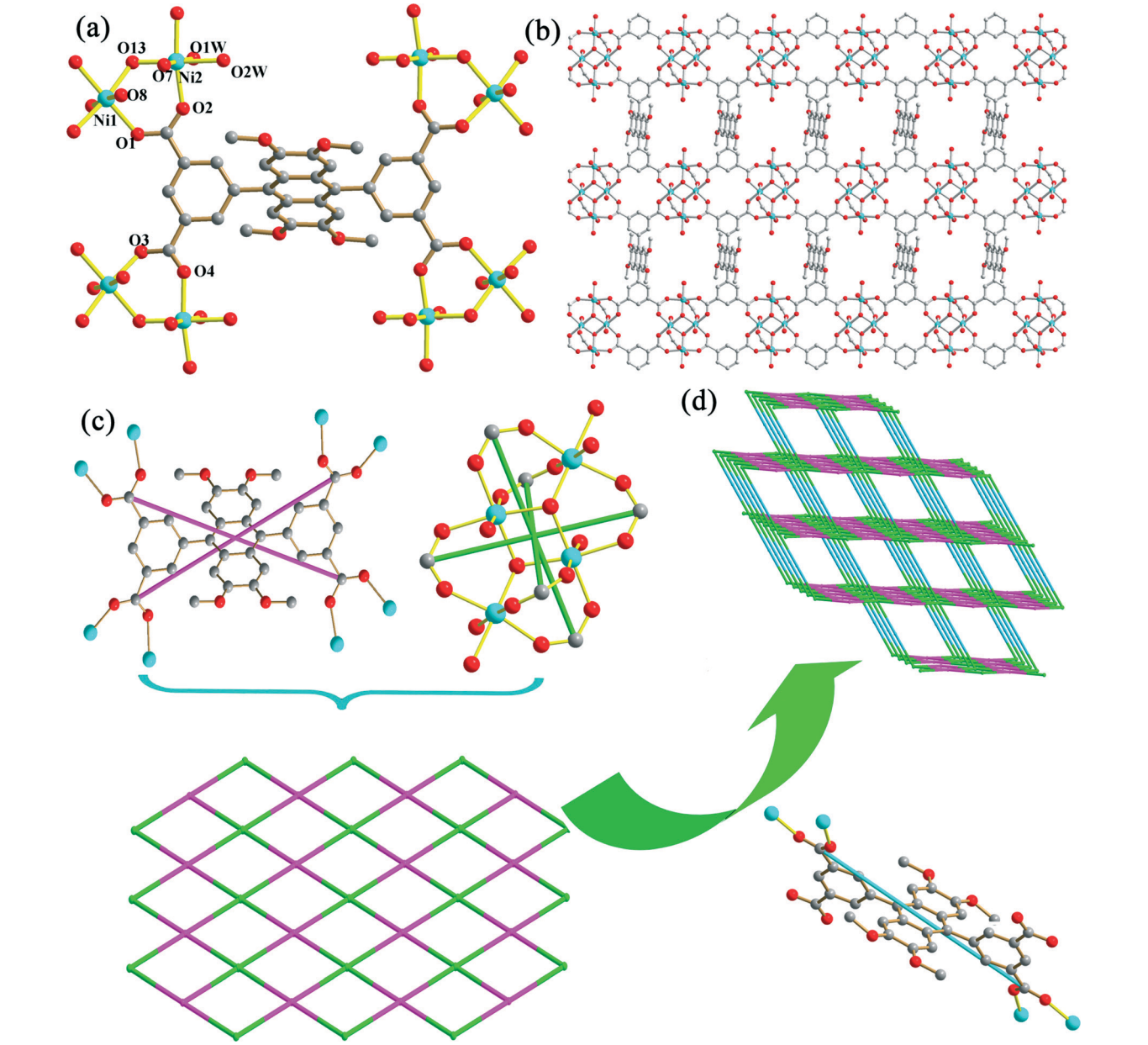

Fig. 2 (a) The coordination environment of Ni(II) ions in **2** (hydrogen atoms omitted for clarity). (b) The 2D layer linked by tetranuclear nickel clusters. (c) Schematic representation of the (4^4)-**sql** layer connected topology. (d) Simplified 3D 2-nodal (4,6)-connected framework. (Symmetry codes: (i) −*x* + 1, −*y* + 2, −*z* + 1; (ii) *x* + 1, *y*, *z*; (iii) −*x*, −*y* + 1, −*z* + 1; (iv) −*x* + 1, −*y* + 1, −*z* + 2; (v) *x* − 1, *y*, *z*).

molecule. Ni2 is bonded to three carboxylate O atoms from three different ligands (Ni2–O2 = 2.027 (3), Ni2–O7 = 2.044 (3), Ni2–O4^{ii} = 2.071 (3) Å), two O atoms from coordinated water molecules and one O atom (Ni2–O13 = 1.975 (2) Å) from μ_3-OH. Similar to **1**, four Ni atoms are linked by six carboxylate groups and two μ_3-OH groups to form tetranuclear nickel units. Complex **2** possesses two types of ligands with different coordination modes: (a) one type is fully deprotonated with μ_8-η^1:η^1:η^1:η^1:η^1:η^1:η^1:η^1 coordination mode; (b) the other type is partly deprotonated with μ_4-η^1:η^1:η^0:η^0:η^1:η^1:η^0:η^0 coordination mode. As shown in Fig. 2b, the tetranuclear units are connected by type (a) ligands to generate a 2D sheet structure, and then the planar 2D layers are further linked by the type (b) ligands to generate a 3D framework. The 3D structure is reinforced by the hydrogen bonds (O3W–H3WB···O7 = 2.860 (5) Å; nonclassical C–H···O) and C–H···π weak interactions. The solvent-accessible void of **2** is about 48.9% (1388.6 Å^3) of the crystal unit cell volume (2838.1 Å^3) by PLATON calculation. In the same way, the topological method is used to simplify the structure in order to clearly understand the complicated architecture. The tetranuclear nickel units are seen as 4-connected nodes, while the L^{OMe} act as 6-connected nodes. Subsequently, the overall 3D framework can be rationalized as a 2-nodal (4,6)-connected framework (Fig. 2c, d) with the Schläfli symbol of $(4^4{\cdot}6^{10}{\cdot}8)(4^4{\cdot}6^2)$.

3.2.3. Structure description of $[Cd_2(L^{OMe})(H_2O)_2(NMP)]$·2DMF·NMP·$H_2O$ (3). X-ray single-crystal diffraction analysis reveals that **3** is a complicated 3D framework with a **PtS** topology. It crystallizes in the monoclinic crystal system with space group $P2_1/c$, and there are two Cd(II) ions, one ligand, two coordinated water molecules and one coordinated NMP in the asymmetric unit. As shown in Fig. 3a, Cd1 has a CdO_7 coordination environment surrounded by seven O atoms from four different ligands. Cd2 displays a distorted octahedral geometry, coordinated by three O atoms from carboxylates of three different ligands, two O atoms from water molecules, and one O atom from NMP. The average Cd–O distance is 2.330 Å, and the O–Cd–O bond angles range from 52.87(9) to 178.21(13)°. In **3**, there are also two types of ligands bearing μ_8-η^1:η^1:η^1:η^2:η^1:η^1:η^1:η^2 and μ_6-η^1:η^1:η^1:η^2:η^1:η^1:η^1:η^2 coordination modes based on different coordination fashions of fully deprotonated carboxylic groups. The ligands bridge dimetal $\{Cd_2O_{11}\}$ units to form a 3D framework, which is further consolidated by hydrogen bonds and π···π stacking interactions. The guest molecules reside in the formed rectangle-like channels, and the solvent-accessible void is

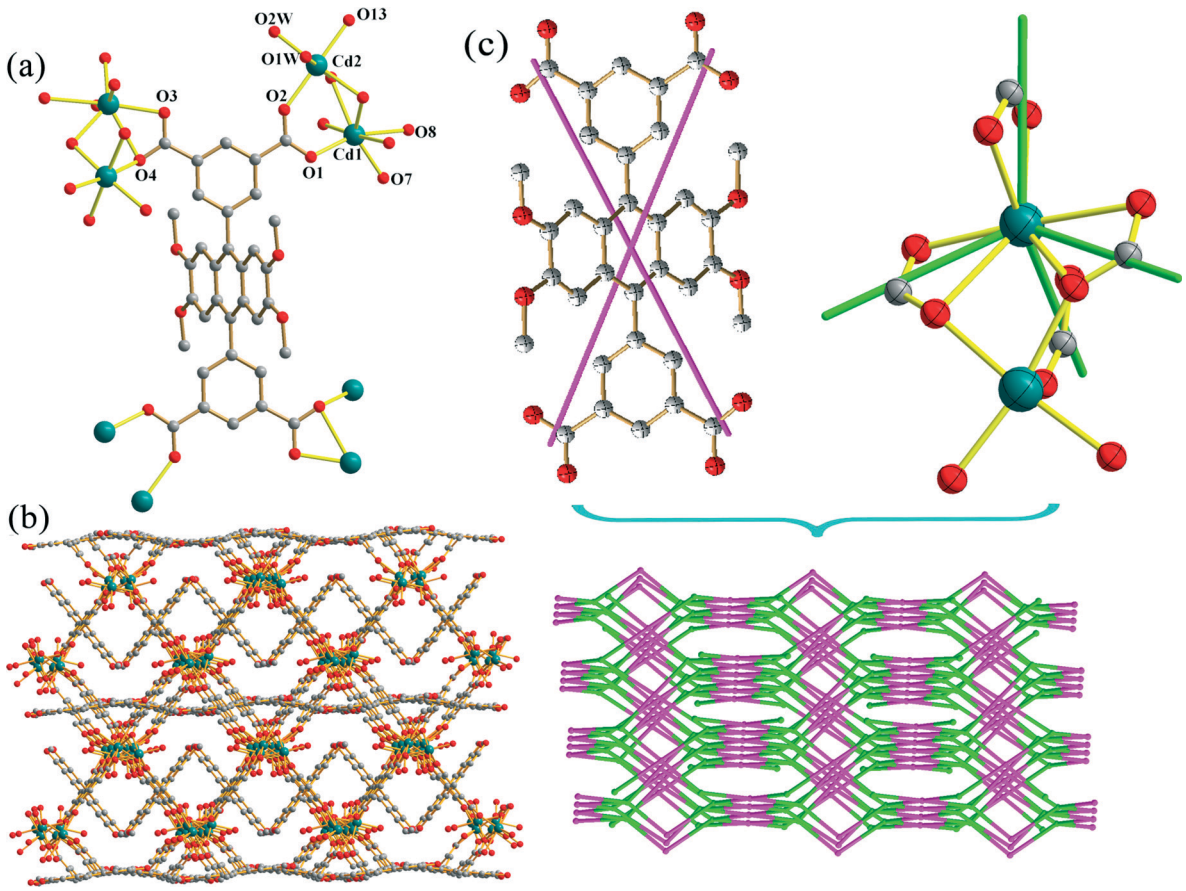

Fig. 3 (a) The coordination environment of Cd(II) ions in **3** (hydrogen atoms omitted for clarity). (b) The 3D net structure of **3**. (c) Simplified 3D 2-nodal (4,4)-connected framework in **3**. (Symmetry codes: (i) −*x* + 1, *y* − 1/2, −*z* + 1/2; (ii) −*x*, *y* + 1/2, −*z* + 1/2; (iii) −*x*, *y* − 1/2, −*z* + 1/2; (iv) −*x* + 1, *y* + 1/2, −*z* + 1/2; (v) −*x*, −*y* + 1, −*z*; (vi) −*x* + 1, −*y* + 2, −*z*).

about 36.6% (1955.4 Å^3) of the crystal unit cell volume (5345.8 Å^3) by PLATON analysis.

A better insight into the nature of this intricate framework can be obtained by using topological analysis. Each dimetal $\{Cd_2O_{11}\}$ cluster can be regarded as a 4-connected node linking four L^{OMe}, and each L^{OMe} can also be simplified as a 4-connected node connecting four dimetal clusters. Hence, the framework structure of **3** can be represented as a cooperite **PtS** net with the Schläfli symbol of $(4^2{\cdot}8^4)$, as displayed in Fig. 3c.

3.2.4. Structure description of $[Co_2(L^{OMe})(H_2O)_2]{\cdot}2NMP{\cdot}DMA{\cdot}2H_2O$ (4) and $[Zn_2(L^{OMe})(H_2O)_2]{\cdot}2NMP{\cdot}2H_2O{\cdot}DOE$ (5). The single-crystal X-ray diffraction studies reveal that the structure of complexes **4** and **5** are very similar. As a representative example, only the crystal structure of **5** is depicted here in detail. It is a 3D framework and crystallizes in the monoclinic $P2_1/c$ space group, and the asymmetric unit consists of two Zn(II) ions, one ligand, two coordinated water molecules, and lattice solvent molecules including two NMP, two water, and one 1,4-dioxane. As illustrated in Fig. 4a, the Zn1 is coordinated to five oxygen atoms from four carboxyl groups of four L^{OMe} ligands, displaying a slightly distorted trigonal bipyramid geometry. The Zn1–O bond lengths fall in the range of 1.944(3)–2.304(3) Å. Zn2 has a distorted square pyramid configuration defined

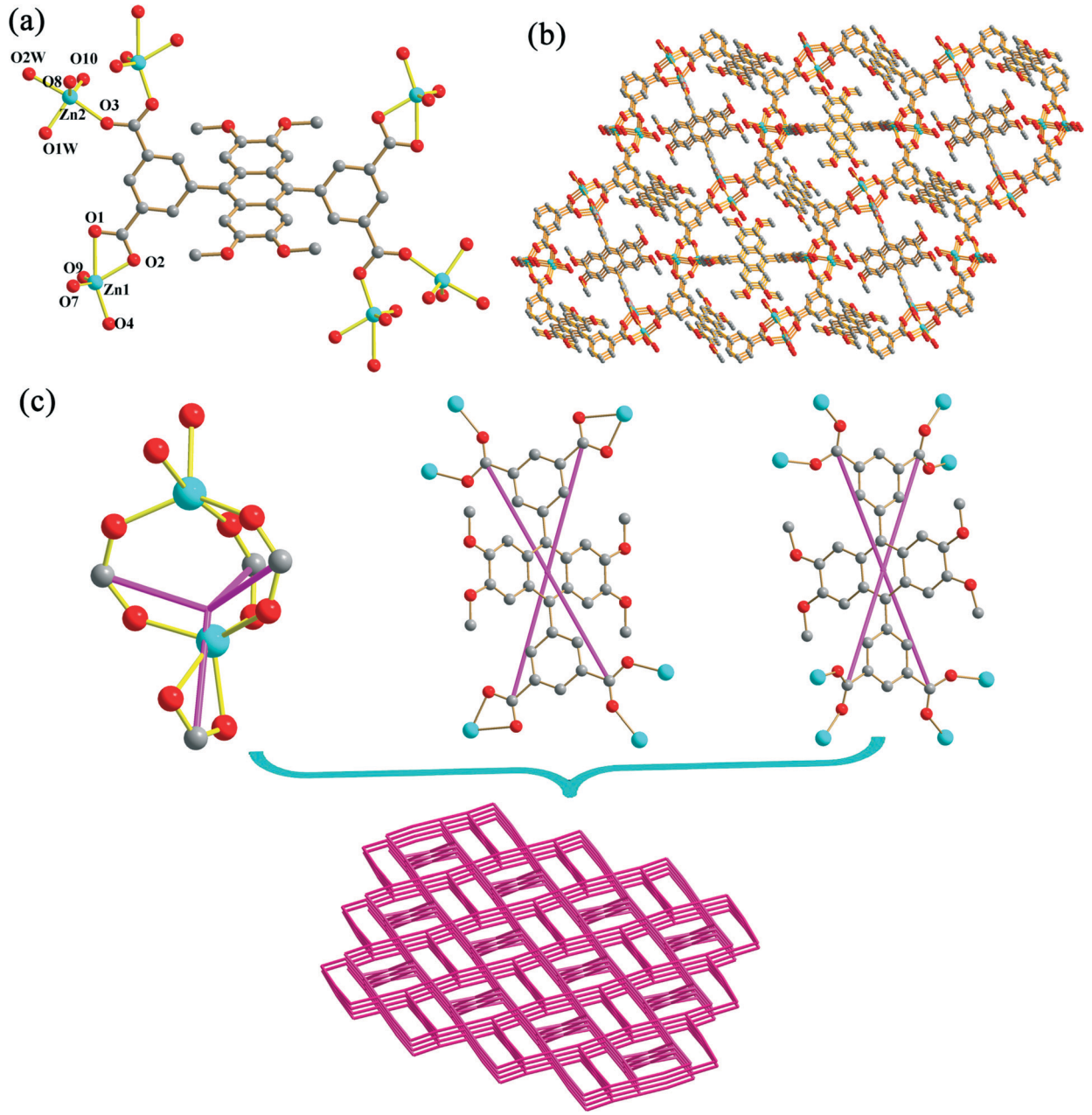

Fig. 4 (a) The coordination environment of Zn(II) ions in **5** (hydrogen atoms omitted for clarity). (b) The 3D net structure of **5**. (c) Simplified 3D 3-nodal (4,4,4)-connected framework. (Symmetry codes: (i) $-x+1, y+1/2, -z+1/2$; (ii) $x+1, y, z$; (iii) $x-1, y, z$; (iv) $-x, -y+2, -z+1$; (v) $-x+1, -y+1, -z+1$; (vi) $-x+1, y-1/2, -z+1$).

by three O atoms from different L^{OMe} ligands (Zn2–O10^{i} = 1.943 (3), Zn2–O8 = 1.945 (3), Zn2–O3^{ii} = 2.062 (3)) and two coordinated water molecules (Zn2–O1W = 1.965 (3), Zn2–O2W = 2.138 (3)). Zn1 and Zn2 are interconnected by carboxylic groups to form a $Zn_2(COO)_4$ unit, which can be simplified as a 4-connected node. The L^{OMe} ligands in **5** display two kinds of coordination modes with μ_8-η^1:η^1:η^1:η^1:η^1:η^1:η^1:η^1 and μ_6-η^1:η^1:η^1:η^1:η^1:η^1:η^1:η^1, respectively, which is different from **2** and **3**. Two types of ligands all coordinate with four inorganic building units, and form two kinds of 4-connected node (Fig. 4c). The assembly of three types of nodes generate a complicated 3-nodal (4,4,4)-connected **nou** network with the symbol of $(4{\cdot}6^5)_2(4^2{\cdot}8^4)(6^4{\cdot}8^2)$, which is rarely reported, although several examples have been referenced to the Reticular Chemistry Structure Resource (RSCR) database.

3.3. Comparison of the crystal structures of 1–5

From a structural description of the above complexes **1–5**, obvious structural diversification is observed from 2D layer to 3D coordination frameworks. We can see that the different coordination geometries of metal ions and the various coordination and conformation modes of ligand are the main reasons for the dramatic structural diversities. In compounds **1–5**, the H_4L^{OMe} ligand adopts five different coordination modes (Scheme 2), which could be subtly sensed by different metal ions. The H_4L^{OMe} ligand has two benzene rings and one anthracene ring which could freely rotate along the C–C bonds to adjust themselves to match with the coordination preferences. Consideration the conformations of H_4L^{OMe}, we defined an important geometric parameter α which represent the dihedral angles between rings A and B (Scheme 2). The details regarding these angles were compiled in Table 3. As is well known, different metal ions usually have preferential coordination geometry depending on their electronic

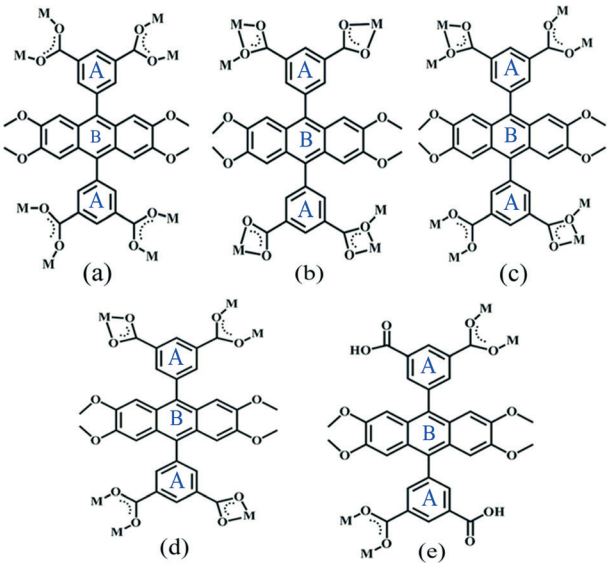

Scheme 2 Coordinate mode of H_4L^{OMe} in **1–5**.

Table 3 Dihedral angles between the anthracene ring and benzene ring in **1–5**

	1	2	3	4	5
α/°	81.3	72.5, 58.4	60.9, 77.5	68.9, 59.5	70.2, 61.9
Coordination modes	(a)	(a), (e)	(b), (c)	(a), (d)	(a), (d)

configurations. In compound **1**, when d^5 Mn^{2+} was added to the system, the ligand only bears one mode (a) while the other complexes contain two types of coordination mode, which is the main reason why it has a 2D metal–organic framework, whereas the others display complicated 3D structures. When d^8 Ni^{2+} was contained in this system, the ligand adopts (a) and (e) coordination modes in compound **2**. For complexes **1** and **2**, both of them possess tetranuclear metal clusters, which are linked by the ligands in mode (a) to generate a 2D structure. In **1**, the metal sites along the axis are occupied by the acetates to prevent the further extension of the layer. However, in **2**, the coordination sites are occupied by the carboxylate groups of the ligands in mode (e) to further link the 2D layer to generate the final 3D framework. When d^{10} Cd^{2+} and d^{10} Zn^{2+} are used in compounds **3** and **5**, respectively, H_4L^{OMe} adopts totally different modes with mode (b), (c) in **3** and mode (a), (d) in **5**. However, when d^7 Co^{2+} and d^{10} Zn^{2+} were used, H_4L^{OMe} ligand displays the same coordination mode (a), (d) with rarely 3-nodal (4,4,4)-connected **nou** network. The results confirm that the various coordination and conformation modes of the organic ligand are influenced not only by coordination geometries of metal ions but also by reaction conditions such as solvent system and temperature. In other words, the ligand can modulate its conformations and coordination modes to fine-tune itself to satisfy the coordination preference of metal centers and the lower energetic arrangement in the assembly process.

3.4. X-ray powder diffraction analyses and thermal analyses

Powder X-ray diffraction (PXRD) has been used to check the phase purity of bulk samples in the solid state. The experimental PXRD patterns correspond well with the results simulated from the single crystal data, indicating the high purity of the synthesized samples. The difference of reflection intensities between the simulated and experimental patterns is due to the variation of preferred orientation of the powder samples during the collection of experimental PXRD data. The thermal behaviors of **1–5** were studied by TGA. The experiments were performed by using the samples consisting of numerous single crystals under N_2 atmosphere with a heating rate of 10 °C min^{-1}, and the TG curves are shown in Fig. S3.†

For complex **1**, a rapid weight loss (obsd 13.3%, calcd 13.1%) appears between room temperature and 150 °C, which is attributed to the removal of water molecules and acetate. Subsequently, the loss of coordination NMP molecules leads to the collapse of the network. Complex **2** has a

rapid weight loss (obsd 11.1%) from room temperature to 75 °C, which accords with the departure of free water molecules (calcd: 11.7%). The curve of **3** shows that the first weight loss of 14.0% happens in the range 27–180 °C, which was thought to be the release of free water molecules and DMF molecules (calcd: 13.58%); and the second weight loss of 15.1% from 180 to 310 °C is ascribed to the loss of NMP molecules (calcd: 15.8%). The framework then collapses and decomposes with the increase of temperature. For **4**, the first loss (obsd 8.64%) from room temperature to 85 °C belongs to the release of one DMA molecule (calcd 7.93%), and the second weight loss (obsd 12.75%) till 247 °C corresponds to the removal of one NMP molecule and two water molecules (calcd: 12.31%), then the main structure rapidly collapses and decomposes. Similarly, complex **5** has a rapid weight loss (obsd 8.95%) till 75 °C, which corresponds to the release of one water molecule and one 1,4-dioxane molecule (calcd: 9.53%), and then the weight continuously decreases to 13.5% (calcd 13.76%) with the loss of one NMP and another three water molecules from 75 to 218 °C. Subsequently, the framework rapidly decomposes.

3.5. Magnetic studies of 1 and 2

The variable-temperature magnetic measurements of complexes **1** and **2** were performed in the temperature range of 1.8–300 K under an applied magnetic field of 1 kOe. The plots of $\chi_M T$ *versus* T together with $1/\chi_M$ *versus* T, where χ_M is the molar magnetic susceptibility per Mn_4 or Ni_4 unit, are shown in Fig. 5(a) and 6(a). The experimental $\chi_M T$ value of **1** at room temperature is 16.36 $cm^3\ mol^{-1}\ K$, which is somewhat lower than the expected value of $\chi_M T = 17.5\ cm^3\ mol^{-1}\ K$ for four $S = 5/2$ uncoupled spins with $g = 2.0$. However, The experimental $\chi_M T$ value of **2** at 300 K is 6.22 $cm^3\ mol^{-1}\ K$, which is slightly larger than the spin value expected for four uncoupled high-spin Ni(II) ions (4 $cm^3\ mol^{-1}\ K$). This could be due to an orbital contribution.[13] The $\chi_M T$ product decreases steadily with the decrease of temperature, and tends to zero at very low temperatures for both complexes due to the Boltzmann depopulation of excited states and population of the ground state, indicating an overall antiferromagnetic behavior. A sharp increase is observed below 50 K for both complexes, which arises from the appearance of canted ferromagnetic interaction between M(II) (Mn or Ni) ions through the oxygen atom of the ligand, as both complexes **1** and **2** have tetranuclear metal clusters, and the angles of Mn–O(H)–Mn and Ni–O(H)–Ni range from 92.85° to 116.11°, and 99.24° to 122.48°, respectively, resulting in competing antiferromagnetic and ferromagnetic interactions. As depicted in Fig. 5(b) and 6(b), the Curie plot shows the change of slope, where the antiferromagnetic coupling dominates in a higher temperature region above 50 K, and the weak ferromagnetic order appears in a lower temperature region owing to the spin-canting reason for **1**. The magnetic susceptibility obeys the Curie–Weiss law down to 100 K with a Curie constant $C = 19.04\ cm^3\ mol^{-1}$ ($1/\chi_M = (T - \theta)/C$) and a Weiss constant $\theta = -48.77$ K for **1**, and down to 25 K with a Curie constant $C = 6.35\ cm^3\ mol^{-1}\ K$ and a Weiss constant $\theta = -18.65$ K for **2**. Negative Weiss constant values indicate predominantly antiferromagnetic coupling down to this temperature.

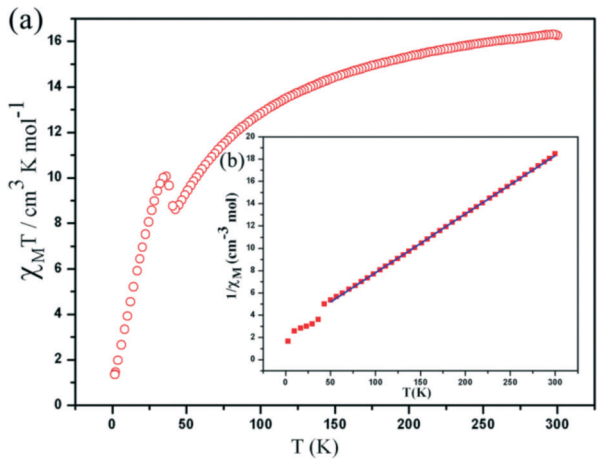

Fig. 5 (a) Experimental magnetic data plotted as $\chi_M T$ *versus* T for complex **1**. (b) The inset showing $1/\chi_M$ *versus* T for complex **1**.

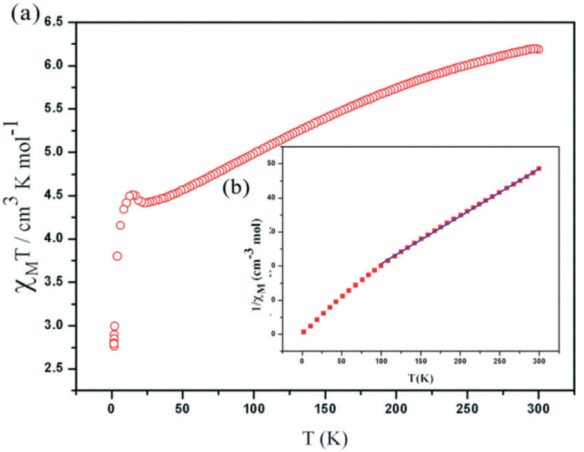

Fig. 6 (a) Experimental magnetic data plotted as $\chi_M T$ *versus* T for complex **2**. (b) The inset showing $1/\chi_M$ *versus* T for complex **2**.

3.6. Photoluminescence properties

Luminescent compounds are of great interest due to their various applications in chemical sensors, photochemistry, and light-emitting diodes (LEDs).[14] The luminescent properties of complexes **1**, **3**, **5** were investigated in the solid state at room temperature as exhibited in Fig. 7. The free ligand H_4L^{OMe} displays photoluminescence with an emission maximum at 467 nm upon 270 nm excitation, which can be attributed to the $\pi^*\cdots\pi$ transition of the p electrons of the aromatic rings. Complexes **1**, **3** and **5** reveal luminescent emission bands at 444 nm (λ_{ex} = 270 nm), 442 nm (λ_{ex} = 290 nm) and 443 nm (λ_{ex} = 300 nm), respectively. When comparing with H_4L^{OMe}, the maximum emission peaks have a blue shift of 23, 22 and 21 nm, respectively. Cd(II) and Zn(II) ions are difficult to

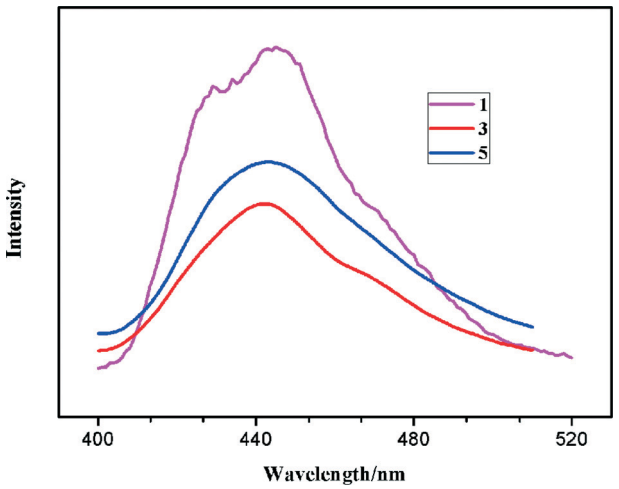

Fig. 7 Photoluminescence of MOFs **1**, **3** and **5**.

oxidize or reduce due to their d^{10} electronic configuration. Hence, their luminescent emissions cannot be assigned to metal-to-ligand charge transfer or ligand-to-metal charge transfer, while they may be tentatively attributed to ligand-based electron transition.[15] However, the chelation of ligand and metal ions may effectively change the dihedral angle between anthracene ring and benzene ring and the angle between the carboxyl plane and benzene ring, and reduce the loss of energy produced from radiationless decay. Therefore, the energy level of the $\pi^*\cdots\pi$ transition is altered, thus further causing the blue shift in **1**, **3** and **5**.

4. Conclusions

In summary, five MOFs based on a newly designed tetracarboxylate ligand were synthesized by changing the reaction conditions including solvents, temperatures, and metal ions, and characterized by elemental analysis, single-crystal X-ray crystallography, powder X-ray diffraction, infrared spectroscopy, and thermogravimetric analyses. Complex **1** bears a 2D layered network with a typical (4,4) topological net; complex **2** reveals a 3D 2-nodal (4,6)-connected **fsc** framework; complex **3** exhibits a 3D 2-nodal (4,4)-connected **PtS** network; complexes **4** and **5** display rare 3D 3-nodal (4,4,4)-connected **nou** structures. Magnetic susceptibility measurement for complexes **1** and **2** confirm the presence of antiferromagnetic coupling at a relatively higher temperature, and ferromagnetic behavior at a lower temperature among the metal ions of tetranuclear clusters. Our investigation not only illustrates that structural diversities of coordination polymers can be achieved by changing the inorganic building unit but also provides new examples of the H_4L^{OMe} ligand for the design of novel frameworks. The compounds containing different transitional metal clusters will enrich the field of coordination polymers based on multicarboxylate ligands. Although several compounds possess high solvent-accessible voids, there are no gas adsorption behaviors due to the blocking of the channels by the coordinated solvates or methoxy substituent. The coordinated solvates on the SBU also decrease the stability of the frameworks. Further studies will focus on the construction of porous frameworks with high thermal stability by use of the H_4L^{OMe} ligand.

Acknowledgements

This work was supported by the NSFC (grant no. 21001115, 21271117), NCET-11-0309 and the Shandong Natural Science Fund for Distinguished Young Scholars (JQ201003), and the Fundamental Research Funds for the Central Universities (13CX05010A, 13CX02006A).

References

1 (*a*) S. Kitagawa, R. Kitaura and S. I. Noro, *Angew. Chem., Int. Ed.*, 2004, **43**, 2334; (*b*) M. Eddaoudi, J. Kim, N. Rosi, D. Vodak, J. Wachter, M. O'Keeffe and O. M. Yaghi, *Science*, 2002, **295**, 469; (*c*) N. W. Ockwig, O. Delgado-Friederichs, M. O'Keeffe and O. M. Yaghi, *Acc. Chem. Res.*, 2005, **38**, 176; (*d*) B. Moulton and M. J. Zaworotko, *Chem. Rev.*, 2001, **101**, 1629.

2 (*a*) O. D. Friedrichs, M. O'Keeffe and O. M. Yaghi, *Acta Crystallogr., Sect. A: Found. Crystallogr.*, 2003, **59**, 22; (*b*) Y. H. Li, C. Y. Su, A. M. Goforth, K. D. Shimizu, K. D. Gray and M. D. Smith, *Chem. Commun.*, 2003, 1360; (*c*) S. A. Bourne, J. Lu, B. Moulton and M. J. Zaworotko, *Chem. Commun.*, 2001, 861; (*d*) X. L. Wang, C. Qin, E. B. Wang, L. Xu, Z. M. Su and C. W. Hu, *Angew. Chem., Int. Ed.*, 2004, **43**, 5036; (*e*) L. Carlucci, G. Ciani, M. Moret, D. M. Proserpio and S. Rizzato, *Angew. Chem., Int. Ed.*, 2000, **39**, 1506; (*f*) X. J. Kong, L. S. Long, Z. Zheng, R. B. Huang and L. S. Zheng, *Acc. Chem. Res.*, 2010, **43**, 201; (*g*) E. B. Rusanov, V. V. Ponomarova, V. V. Komarchuk, H. Stoeckli-Evans, E. Fernandez-Ibanez, F. Stoeckli, J. Sieler and K. V. Domasevitch, *Angew. Chem., Int. Ed.*, 2003, **42**, 2499; (*h*) D. Zhao, S. W. Tan, D. Q. Yuan, W. G. Lu, Y. H. Rezenom, H. L. Jiang, L. Q. Wang and H. C. Zhou, *Adv. Mater.*, 2011, **23**, 90; (*i*) B. Chen, S. Xiang and G. Qian, *Acc. Chem. Res.*, 2010, **43**, 1115.

3 (*a*) D. F. Sun, S. Q. Ma, Y. X. Ke, D. J. Collins and H. C. Zhou, *J. Am. Chem. Soc.*, 2006, **128**, 3896; (*b*) K. V. Domasevitch, P. V. Solntsev, I. A. Gural'skiy, H. Krautscheid, E. B. Rusanov, A. N. Chernega and J. A. K. Howard, *Dalton Trans.*, 2007, 3893; (*c*) D. Q. Yuan, D. Zhao, D. F. Sun and H. C. Zhou, *Angew. Chem., Int. Ed.*, 2010, **49**, 5357; (*d*) C. Y. Su, Y. P. Cai, C. L. Chen, M. D. Smith, W. Kaim and H. C. Zur Loye, *J. Am. Chem. Soc.*, 2003, **125**, 8595; (*e*) J. J. Perry, J. A. Perman and M. J. Zaworotko, *Chem. Soc. Rev.*, 2009, **38**, 1400; (*f*) K. K. Tanabe, C. A. Allen and S. M. Cohen, *Angew. Chem., Int. Ed.*, 2010, **49**, 9730; (*g*) B. Moulton and M. J. Zaworotko, *Chem. Rev.*, 2001, **101**, 1629; (*h*) Z. Yin, Q. X. Wang and M. H. Zeng, *J. Am. Chem. Soc.*, 2012, **134**, 4857; (*i*) M. H. Zeng, W. X. Zhang, X. Z. Sun and X. M. Chen, *Angew.*

Chem., Int. Ed., 2005, **44**, 3079; (*j*) D. Zhao, D. Q. Yuan, D. F. Sun and H. C. Zhou, *J. Am. Chem. Soc.*, 2009, **131**, 9186; (*k*) Y. F. Bi, X. T. Wang, W. P. Liao, X. F. Wang, X. W. Wang, H. J. Zhang and S. Gao, *J. Am. Chem. Soc.*, 2009, **131**, 11650; (*l*) X. P. Zhou, M. Li, J. Liu and D. Li, *J. Am. Chem. Soc.*, 2012, **134**, 67; (*m*) X. P. Zhou, J. Liu, S. Z. Zhan, J. R. Yang, D. Li, K. M. Ng, R. W. Y. Sun and C. M. Che, *J. Am. Chem. Soc.*, 2012, **134**, 8042; (*n*) J. H. Fu, H. J. Li, Y. J. Mu, H. W. Hou and Y. T. Fan, *Chem. Commun.*, 2011, **47**, 5271; (*o*) M. H. Zeng, Q. X. Wang, Y. X. Tan, S. Hu, H. X. Zhao, L. S. Long and M. Kurmoo, *J. Am. Chem. Soc.*, 2010, **132**, 2561; (*p*) D. Sun, D. F. Wang, X. G. Han, N. Zhang, R. B. Huang and L. S. Zheng, *Chem. Commun.*, 2011, **47**, 746.

4 (*a*) C. N. Morrison, A. K. Powell and G. E. Kostakis, *Cryst. Growth Des.*, 2011, **11**, 3653; (*b*) R. Cao, D. F. Sun, Y. C. Liang, M. C. Hong, K. Tatsumi and Q. Shi, *Inorg. Chem.*, 2002, **41**, 2087; (*c*) P. Mahata and S. Natarajan, *Inorg. Chem.*, 2007, **46**, 1250; (*d*) O. M. Yaghi, M. O'Keeffe, N. W. Ockwig, H. K. Chae, M. Eddaoudi and J. Kim, *Nature*, 2003, **423**, 705; (*e*) D. L. Reger, R. P. Watson and M. D. Smith, *Inorg. Chem.*, 2006, **45**, 10077; (*f*) C. Tedesco, L. Erra, I. Immediata, C. Gaeta, M. Brunelli, M. Merlini, C. Meneghini, P. Pattison and P. Neri, *Cryst. Growth Des.*, 2010, **10**, 1527; (*g*) D. N. Dybtsev, H. Chun and K. Kim, *Chem. Commun.*, 2004, 1594; (*h*) Y. B. Dong, H. X. Xu, J. P. Ma and R. Q. Huang, *Inorg. Chem.*, 2006, **45**, 3325; (*i*) N. Ishii, J. I. Mamiya, T. Ikeda and F. M. Winnik, *Chem. Commun.*, 2011, **47**, 1267; (*j*) D. Sun, F. J. Liu, R. B. Huang and L. S. Zheng, *Inorg. Chem.*, 2011, **50**, 12393; (*k*) N. Ishii, J. I. Mamiya, T. Ikeda and F. M. Winnik, *Chem. Commun.*, 2011, **47**, 1267; (*l*) D. Sun, S. Yuan, H. Wang, H. F. Lu, S. Y. Feng and D. F. Sun, *Chem. Commun.*, 2013, **49**, 6152.

5 (*a*) D. Sun, F. J. Liu, R. B. Huang and L. S. Zheng, *CrystEngComm*, 2013, **15**, 1185; (*b*) N. L. Torad, M. Hu, Y. Kamachi, K. Takai, M. Imura, M. Naito and Y. Yamauchi, *Chem. Commun.*, 2013, **49**, 2521; (*c*) D. Sun, Z. H. Yan, M. Liu, H. Xie, S. Yuan and H. F. Lu, *Cryst. Growth Des.*, 2012, **12**, 2902; (*d*) M. Hu, A. A. Belik, M. Imura and Y. Yamauchi, *J. Am. Chem. Soc.*, 2013, **135**, 384.

6 (*a*) B. L. Chen, N. W. Ockwig, A. R. Millward, D. S. Contreras and O. M. Yaghi, *Angew. Chem., Int. Ed.*, 2005, **44**, 4745; (*b*) X. Lin, I. Telepeni, A. J. Blake, A. Dailly, C. M. Brown, J. M. Simmons, M. Zoppi, G. S. Walker, K. M. Thomas, T. J. Mays, P. Hubberstey, N. R. Champness and M. Schröder, *J. Am. Chem. Soc.*, 2009, **131**, 2159; (*c*) H. S. Choi and M. P. Suh, *Angew. Chem., Int. Ed.*, 2009, **48**, 6865; (*d*) X. T. Zhang, L. M. Fan, Z. Sun, W. Zhang, D. C. Li and J. M. Dou, *Cryst. Growth Des.*, 2013, **13**, 792.

7 (*a*) D. R. Xiao, Y. G. Li, E. B. Wang, L. L. Fan, H. Y. An, Z. M. Su and L. Xu, *Inorg. Chem.*, 2007, **46**, 4158; (*b*) J. M. Lim, P. Kim, M. C. Yoon, J. Sung, V. Dehm, Z. J. Chen, F. Wurthner and D. Kim, *Chem. Sci.*, 2013, **4**, 388; (*c*) F. Guo, F. Wang, H. Yang, X. L. Zhang and J. Zhang, *Inorg. Chem.*, 2012, **51**, 9677; (*d*) H. L. Tsai, C. I. Yang, W. Wernsdorfer, S. H. Huang, S. Y. Jhan, M. H. Liu and G. H. Lee, *Inorg. Chem.*, 2012, **51**, 13171.

8 (*a*) Y. G. Lee, H. R. Moon, Y. E. Cheon and M. P. Suh, *Angew. Chem., Int. Ed.*, 2008, **47**, 7741; (*b*) X. Lin, J. H. Jia, X. Zhao, K. M. Thomas, A. J. Blake, G. S. Walker, N. R. Champness, P. Hubberstey and M. Schröder, *Angew. Chem., Int. Ed.*, 2006, **45**, 7358; (*c*) B. L. Chen, N. W. Ockwig, A. R. Millward, D. S. Contreras and O. M. Yaghi, *Angew. Chem., Int. Ed.*, 2005, **44**, 4745; (*d*) B. Zheng, J. H. Luo, F. Wang, Y. Peng, G. H. Li, Q. H. Huo and Y. L. Liu, *Cryst. Growth Des.*, 2013, **13**, 1033.

9 G. M. Sheldrick, *SHELXS-97, Program for X-ray Crystal Structure Determination*, University of Gottingen, Gottingen, Germany, 1997.

10 G. M. Sheldrick, *SHELXL-97, Program for X-ray Crystal Structure Refinement*, University of Gottingen, Gottingen, Germany, 1997.

11 A. L. Spek, *Implemented as the PLATON Procedure, a Multipurpose Crystallographic Tool*, Utrecht University, Utrecht, The Netherlands, 1998.

12 (*a*) S. O. H. Gutschke, M. Molinier, A. K. Powell, R. E. P. Winpenny and P. T. Wood, *Chem. Commun.*, 1996, 823; (*b*) D. Sun, M. Z. Xu, S. S. Liu, H. F. Lu, S. Y. Feng and D. F. Sun, *Dalton Trans.*, 2013, **42**, 12324.

13 J. S. Miller and A. J. Epstein, *Angew. Chem., Int. Ed. Engl.*, 1994, **33**, 385.

14 (*a*) X. Li, H. L. Sun, X. S. Wu, X. Qiu and M. Du, *Inorg. Chem.*, 2010, **49**, 1865; (*b*) J. S. Hu, Y. J. Shang, X. Q. Yao, L. Qin, Y. Z. Li, Z. J. Guo, H. G. Zheng and Z. L. Xue, *Cryst. Growth Des.*, 2010, **10**, 2676.

15 (*a*) S. J. Wang, S. S. Xiong, Z. Y. Wang and J. F. Du, *Chem.–Eur. J.*, 2011, **17**, 8630; (*b*) D. Sun, C. F. Yang, H. R. Xu, H. X. Zhao, Z. H. Wei, N. Zhang, L. J. Yu, R. B. Huang and L. S. Zheng, *Chem. Commun.*, 2010, **46**, 8168; (*c*) D. Sun, Z. H. Yan, Y. K. Deng, S. Yuan, L. Wang and D. F. Sun, *CrystEngComm*, 2012, **14**, 7856; (*d*) M. D. Allendorf, C. A. Bauer, R. K. Bhaktaa and R. J. T. Houka, *Chem. Soc. Rev.*, 2009, **38**, 1330.

